

CrossMark
click for updatesCite this: *J. Mater. Chem. A*, 2016, 4, 7245

Monolithic-structured ternary hydroxides as freestanding bifunctional electrocatalysts for overall water splitting†

Xiaolin Zhu,^{ab} Cheng Tang,^a Hao-Fan Wang,^a Bo-Quan Li,^a Qiang Zhang,^{*a} Chunyi Li,^b Chaohe Yang^b and Fei Wei^a

Efficient oxygen and hydrogen evolution electrocatalysts, based on low-cost and earth-abundant elements, are strongly required for sustainable hydrogen production through water splitting. Herein, we fabricated a monolithic-structured electrode by facilely electrodepositing NiCoFe ternary layered double hydroxides (LDHs) onto 3D conductive scaffolds, providing abundant fully exposed active sites for electrochemical reactions. The moderate Co dopant effectively improved the electrical conductivity of the LDH phase and substantially increased its intrinsic activity. When used for oxygen evolution, the as-obtained monolith LDH electrode exhibited superior kinetics with 275 mV overpotential required to achieve 10 mA cm⁻² in 0.10 M KOH, as well as a very low activation energy of 21.0 kJ mol⁻¹. Such a freestanding electrode was also able to catalyze hydrogen evolution efficiently in alkaline media, which further enabled a high-efficiency water electrolyzer delivering 10 mA cm⁻² at a very low cell voltage of 1.62 V in 1.0 M KOH. This sheds fresh insight into the principle and process of practical water electrolysis through the rational design of precious-metal-free bifunctional electrodes with a monolithic configuration.

Received 15th March 2016

Accepted 10th April 2016

DOI: 10.1039/c6ta02216b

www.rsc.org/MaterialsA

1. Introduction

Water electrolysis is widely considered as a critical process for sustainable hydrogen production and renewable energy storage.¹ The renewable energy resources (e.g., sunlight, wind, and wave power) can be converted to clean hydrogen fuel through water splitting, effectively addressing the issues of storage and transport. However, the practical application of water electrolysis is strongly limited by the sluggish kinetics of oxygen evolution reaction (OER) and hydrogen evolution reaction (HER).² For instance, a cell voltage up to 1.8–2.0 V, much higher than the theoretical value of 1.23 V, is typically used in the commercial electrolyzers, which calls for efficient catalysts to expedite both reactions and reduce the overpotential.³ The state-of-the-art catalysts to split water are IrO₂/RuO₂ for OER and Pt alloys for HER respectively,⁴ both of which suffer from scarcity and high cost. Recently, a great deal of efforts have been made in exploring non-precious metal catalysts, such as doped carbon,⁵ transition metal oxides^{6,7}/hydroxides,⁸ and perovskite

oxides⁹ for OER, and metal chalcogenides,¹⁰ carbides,¹¹ and phosphides¹² for HER. Whereas, it is extremely difficult to couple OER and HER in an integrated electrolyzer due to the mismatch of pH ranges for these catalysts to be stable and active.¹³ Therefore, new insight into a bifunctional electrocatalyst for both OER and HER in exactly the same electrolyte is very important and necessary.

Layered double hydroxides (LDHs), as a typical class of two-dimensional materials, have attracted increasing attention in electrocatalysis due to their tunable composition, unique structure, and large specific surface area.¹⁴ Various binary catalyst systems (e.g., NiFe,¹⁵ NiCo,¹⁶ CoFe,¹⁷ and CoMn¹⁸ LDHs) have been explored for OER, but the extremely low conductivity of LDHs seriously hinders the electron transfer and degrades the electrocatalytic performance.¹⁹ Recently, the introduction of a ternary dopant (e.g., Co²⁰ and Mn²¹) into the NiFe LDH phase is reported to lead to a more conductive electronic structure and enhanced electrocatalytic activity. In this regard, the ternary NiCoFe LDHs are selected as the active phase to fabricate the electrocatalyst in this work. Although various nanocarbon materials (e.g., carbon nanotubes,²² graphene,²³ and carbon quantum dots²⁴) have been hybridized with LDHs to further improve the conductivity, the resultant composites are inevitable to aggregate due to their nano-sized nature, and the lack of long-range ordered structure also restricts the increase of surface active sites and the charge-transfer process.

When the active phases are uniformly deposited on a 3D macroporous conductive framework, both the liquid reactants

^aBeijing Key Laboratory of Green Chemical Reaction Engineering and Technology, Department of Chemical Engineering, Tsinghua University, Beijing 100084, PR China. E-mail: zhang-qiang@mails.tsinghua.edu.cn

^bState Key Laboratory of Heavy Oil Processing, China University of Petroleum, Qingdao 266580, PR China

† Electronic supplementary information (ESI) available: SEM and TEM images, XRD patterns, N₂ adsorption-desorption isotherms, and OER activities of different samples, as well as a series of supplementary tables. See DOI: 10.1039/c6ta02216b

and gas products can be rapidly diffused during water splitting, and the sluggish electrochemical reactions can also be accelerated by adequate exposure of active sites. On this basis, we proposed a monolithic-structured electrocatalyst with in situ electrodeposited ternary NiCoFe LDH thin films onto 3D conductive Ni foam (NF). In the as-obtained NiCoFe/NF complex, the mesoporous LDH arrays afford abundant fully exposed and highly active sites for OER and HER, while the NF substrate serves as not only a current collector, but also a smooth diffusion path for gaseous products. This free-standing NiCoFe/NF electrode was demonstrated to exhibit outstanding OER and HER bifunctional performance in an alkaline electrolyte, with a low cell voltage of 1.62 V to achieve 10 mA cm^{-2} water-splitting current in 1.0 M KOH.

2. Results and discussion

Structure of the NiCoFe/NF electrode

The NiCoFe/NF monolith electrode was prepared by co-electrodeposition of Ni, Co, and Fe hydroxides onto a NF substrate. The scanning electron microscopy (SEM) images of the resultant NiCoFe/NF complex (Fig. 1a–c) indicate that the electrodeposited NiCoFe LDH nanoplates are uniformly dispersed over the 3D conductive NF scaffolds, constituting a mesoporous thin film. When taken for OER and HER, the well-arranged NiCoFe LDHs supply abundant highly accessible active centers for these heterogeneous surface reactions. Meanwhile, such uniform packing of LDHs endows the monolith structure with a super-aerophobic surface retarding the formation of large gas

bubbles,²⁵ and the plentiful macropores in the NF framework further facilitate the rapid diffusion of O_2 and H_2 bubbles yielded.

The ultrathin hexagonal NiCoFe LDH sheets with a lateral size of ca. 100 nm appear to be highly transparent under transmission electron microscopy (TEM) (Fig. 1d). The corresponding energy dispersive spectroscopy (EDS) mapping (Fig. 1e) indicates a homogeneous distribution of Ni, Co, and Fe elements throughout these LDH plates. X-ray diffraction (XRD) patterns (Fig. 1f) further demonstrate that the electrodeposited NiCoFe LDHs are well crystallized with a group of hydroxal-cite-like characteristic (003), (006), (012), and (110) peaks. The 0.25 nm fringe spacing of the LDH plates (the inset in Fig. 1d) is in good accordance with the (012) lattice plane.

Such tri-metallic composition of the NiCoFe LDHs is also confirmed by X-ray photoelectron spectroscopy (XPS). Two spin-orbit peaks are fitted in the Ni 2p spectrum (Fig. 1g), namely Ni 2p_{3/2} and Ni 2p_{1/2} at 855.5 and 873.2 eV, which are consistent with the Ni(OH)₂ phase and suggested a Ni²⁺ oxidation state of Ni.^{7,26} The Co 2p spectrum exhibits Co 2p_{3/2} and Co 2p_{1/2} peaks at 780.9 and 796.5 eV, respectively, indicating that Co is mostly in an oxidation state of Co²⁺.²⁷ The Fe 2p_{3/2} and Fe 2p_{1/2} peaks centered at 711.1 and 724.4 eV in the Fe 2p spectrum are further assigned to the Fe³⁺ oxidation state.²⁸

Combining the results of SEM, TEM, EDS, XRD, and XPS, we confirm that ternary LDH thin films are uniformly decorated over NF scaffolds in the monolith catalyst. Furthermore, we should notice that the electrodeposition method is a general strategy to achieve monolithic-structured catalysts, as verified by the NiFe/NF complex (Fig. S1 in the ESI†) fabricated using a precursor solution without Co nitrate.

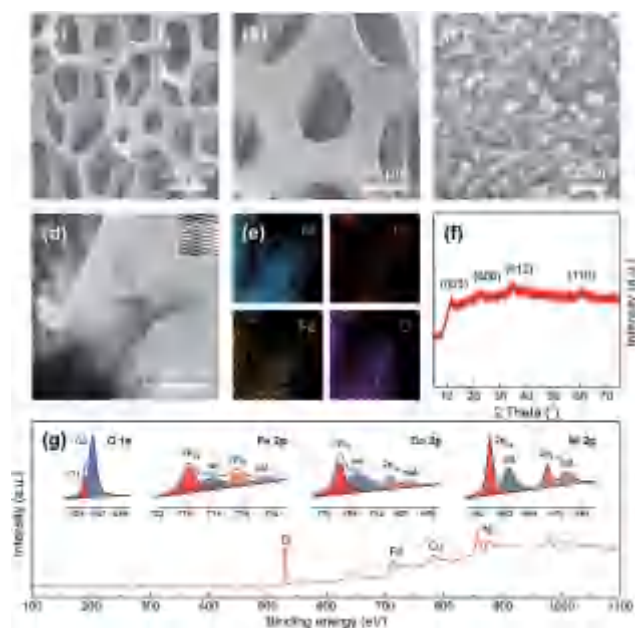


Fig. 1 Morphology and structure characterizations of a NiCoFe/NF monolith electrode. (a–c) SEM images of the freestanding NiCoFe/NF electrode. (d) TEM image and (e) corresponding EDS mapping of the electrodeposited NiCoFe LDH. (f) XRD pattern of NiCoFe LDH. (g) XPS survey as well as high-resolution O, Fe, Co, and Ni spectra of NiCoFe LDH.

OER and HER bifunctional performance

A series of monolithic-structured electrodes were prepared through facile electrodeposition in electrolytes of different compositions, with the resultant complexes (e.g., Ni₃Fe/NF, Ni_{2.5}Co_{0.5}Fe/NF, and Ni₂CoFe/NF) being named following the metal ion ratio of precursors. Here, the molar ratio of Ni and Co to Fe ions in precursor electrolytes was maintained at 3, based on the reported compositions for the NiFe LDH phase to deliver a decent electrocatalytic activity.^{7,29} The OER and HER performance was comparatively tested in a N₂-saturated 0.10 M KOH solution on a three-electrode system. The electrochemical activity was evaluated by iR-corrected linear sweep voltammetry (LSV) curves collected on the reversible hydrogen electrode (RHE) scale at a scan rate of 10 mV s⁻¹. Compared with the bare NF, the complexes with electrodeposited thin films of ternary LDHs deliver a much lower onset potential and higher OER and HER current densities (Fig. 2a and c), indicating a significantly enhanced bifunctional reactivity. The horizontal dotted line in Fig. 2a represents the overpotential required to reach a current density of 10 mA cm^{-2} (η_{10}), which corresponds to 10% efficient solar water-splitting devices and is usually regarded as a critical parameter for OER.³⁰ As for Ni_{2.5}Co_{0.5}Fe/NF, a η_{10} of 275 mV is achieved, which is ca. 160 mV lower than that of bare NF and also outperforms Ni₃Fe/NF with ca. 30 mV decreased

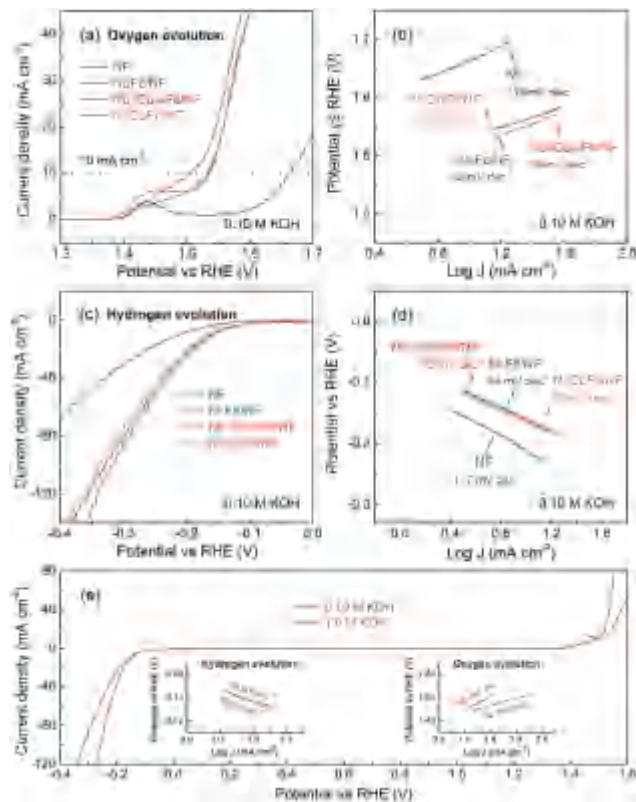


Fig. 2 Bifunctional catalytic performance of a NiCoFe/NF electrode in a 0.10 M KOH electrolyte. (a) LSV curves and (b) corresponding Tafel plots for OER. (c) LSV curves and (d) corresponding Tafel plots for HER. (e) Reactivity of the $\text{Ni}_{2.5}\text{Co}_{0.5}\text{Fe}/\text{NF}$ electrode obtained in 0.10 and 1.0 M KOH solutions, with the insets showing the Tafel plots.

overpotential. Likewise, the $\text{Ni}_{2.5}\text{Co}_{0.5}\text{Fe}/\text{NF}$ electrode affords an outstanding HER activity as well (Fig. 2c).

The promoting effect of Co doping on enhancing the catalytic activity of NiFe LDHs was also experimentally confirmed in this work. Among the recently reported NiFe-based catalysts for OER, the NiCoFe/NF herein exhibits a much lower η_{10} than the average level around 340 mV, and also delivers the highest current density up to 60 mA cm^{-2} at 400 mV overpotential (Table S1†). Moreover, given the fact that the HER activity in an alkaline solution is typically 2–3 orders lower than that in an acidic solution, the performance of NiCoFe/NF is regarded as remarkable.^{31,32}

The superior bifunctional performance is also reflected by the Tafel plots (Fig. 2b and d). After deposition of ternary LDHs onto the bare NF, the Tafel slope is reduced by ca. 20 mV dec^{-1} for both OER and HER, suggesting a significantly boosted current density over the deposited complexes at higher overpotentials. When subjected to a 1.0 M KOH electrolyte, the bifunctional catalytic performance is further enhanced, with both a higher current density and lower Tafel slope (Fig. 2e). Specifically, the potentials required to deliver 40 mA cm^{-2} current over $\text{Ni}_{2.5}\text{Co}_{0.5}\text{Fe}/\text{NF}$ are reduced to 1.54 V for OER and -0.20 V for HER, both much lower than the reported values over Pt loaded on NF (ca. 1.66 and -0.24 V).³² Meanwhile, the Tafel slopes decrease to 52 and 78 mV dec^{-1} for OER and HER

respectively, indicating much enhanced kinetics in a concentrated electrolyte.

Insight into the superior electrocatalytic activity

To confirm the promoting phenomena of Co doping in ternary LDHs for electrocatalysis, a series of NiCoFe LDH samples were synthesized by a routine hydrothermal method for direct analysis of the LDH phases. The as-obtained LDHs are well crystallized (Fig. S2†), and their elemental compositions are close to those of the electrodeposited LDH samples (Table S2†). Compared with binary NiFe LDHs, the ternary LDHs afford a lower specific surface area (Fig. S3a†) due to their larger plate size; however, they deliver higher OER activity and lower onset potential than the binary LDHs (i.e., Ni_3Fe LDHs) (Fig. 3a). When the current density is normalized to the catalyst surface area, the gap between the activities of ternary and binary LDHs is further enlarged (Fig. S3b†). Notably, due to the absence of NF with inevitable surface NiO species, the strong redox peak primarily attributed to the oxidation of NiO to NiOOH (Fig. 2a) is not detected here.

To further probe the role of Co doping, an electrochemical impedance spectroscopy (EIS) test was carried out (Fig. 3b). The ternary LDHs render a smaller charge transfer resistance than the binary LDHs, as revealed by the reduced semicircle diameter in the high frequency range of the Nyquist plot. This is attributed to the fact that the formation of CoOOH through $\text{Co}(\text{OH})_2$ oxidation facilitates the electron transport and proton migration over the $\text{Ni}(\text{OH})_2$ electrode, and consequently increases the electrode utilization and electrochemical activity.³³ This improved conductivity corresponds to a more conductive

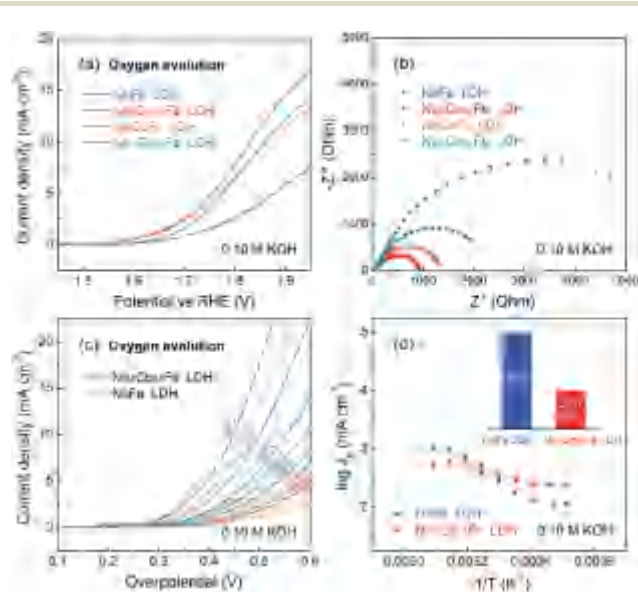


Fig. 3 Enhanced electrocatalytic activity of ternary LDHs arising from Co doping. (a) LSV curves of NiCoFe LDHs with different compositions in 0.10 M KOH. (b) Nyquist plots of NiCoFe LDHs obtained from EIS measurement. (c) LSV curves of $\text{Ni}_{2.5}\text{Co}_{0.5}\text{Fe}$ LDH and Ni_3Fe LDH at various temperatures in 0.10 M KOH. (d) Arrhenius plots of the exchange current density J_0 against the inverse temperature $1/T$, and the inset gives the calculated OER activation energy.

electronic structure stemming from the synergy of multiple transition metals present.^{20,21} However, too much Co dopant degrades the performance in contrast on Ni₂CoFe and Ni_{1.5}-Co_{1.5}Fe LDH electrocatalysts. This degraded performance is mainly attributed to the increasing charge transfer resistance (Fig. 3b), which results from the weakened synergistic effect at higher dopant amounts.

We also determined the apparent activation energy of OER to quantitatively describe the kinetic behavior on ternary LDHs. The activation energy was calculated based on LSV measurements at various temperatures (Fig. 3c). Apparently, the increase in temperature induces an obvious shift of the LSV curves to lower overpotentials (ca. 35 mV of η_{10} is reduced for each 5 °C gradient), providing direct evidence of the effect of temperature. Herein, the exchange current density at each temperature is determined by the equation of the Tafel slope (Table S3†), and then the activation energy is computed from the Arrhenius plots (Fig. 3d).³⁴ Compared with Ni₃Fe LDH (52.3 kJ mol⁻¹), the activation energy of Ni_{2.5}Co_{0.5}Fe LDH is significantly reduced to 21.0 kJ mol⁻¹. Such a low activation energy on ternary LDHs even approaches the reported record for IrO₂ (ca. 16 kJ mol⁻¹),³⁵ and directly verifies the importance of Co doping. In essence, it is exactly the improved electrical conductivity due to Co dopants that reduces the activation energy and substantially enhances the intrinsic electrochemical reactivity of the ternary LDH phase.

Considering the outstanding bifunctional performance of NiCoFe/NF for OER and HER in alkaline media, a two-electrode electrolyzer was assembled by pairing Ni_{2.5}Co_{0.5}Fe/NF as both anode and cathode in a 1.0 M KOH electrolyte (Fig. 4a). The Ni_{2.5}Co_{0.5}Fe/NF affords 10 mA cm⁻² water-splitting current at only a cell voltage of 1.62 V (Fig. 4b), distinctly outperforming the electrolyzers based on Ni(OH)₂/NF (1.82 V), NiFe LDH/NF (1.70 V) and even Pt/C on NF (1.67 V).³² In contrast to the latest bifunctional catalysts reported, a comparable cell voltage at 10 mA cm⁻² is achieved on this complex but with a much lower catalyst loading (Table S4†), fully demonstrating the significance of the fully exposed and highly active NiCoFe LDHs on NF scaffolds. Moreover, 87% preservation of initial current density around 10 mA cm⁻² is observed after a 10 000 s test (Fig. S4†), indicating a good stability of monolith ternary LDHs for overall

water splitting. During water electrolysis, plentiful O₂ and H₂ bubbles are released from the surface of both electrodes respectively (Movie S1†). Meanwhile, the pristine gray-colored electrode turns to dark black on the anodic side, which is mainly attributed to the oxidation of transparent Ni²⁺ to black Ni³⁺.³⁶ To sum up, the decent bifunctionality, high activity, facile preparation, and low cost of the NiCoFe/NF electrode make it an extremely competitive electrocatalyst for practical applications in water electrolysis.

3. Conclusions

A monolith-structured electrocatalyst with ternary LDHs decorated on 3D conductive NF was proposed and validated for overall water splitting. On one hand, the NF host affords a long-range ordered porous framework, facilitating both the macroscopic charge transport and gas diffusion. On the other hand, NiCoFe LDHs constitute a well-arranged thin film on the NF surface, providing abundant highly accessible active sites and superhydrophobic surface retarding the formation of large gas bubbles. The Co dopants effectively improve the conductivity of ternary LDHs, further enhancing their intrinsic reactivity for OER/HER. Therefore, the monolith NiCoFe/NF exhibited superb OER and HER activities in alkaline media with an extremely low activation energy of 21.0 kJ mol⁻¹, and the water electrolyzer pairing NiCoFe/NF as both anode and cathode was able to achieve 10 mA cm⁻² at a very low cell voltage of 1.62 V. This sheds fresh insight into the principle and process of practical water electrolysis through the rational design of precious-metal-free bifunctional electrodes with a monolithic configuration.

4. Experimental section

Material synthesis

Preparation of a NiCoFe/NF electrode. The NiCoFe/NF electrode was fabricated following an electrodeposition method. Typically, Ni foam (NF) with 20 mm × 10 mm × 1.5 mm size was sonicated in a 2.0 M HCl solution, deionized water and ethanol each for 15 min to clean the surface, and then left to dry in air. The electrodeposition was conducted in a standard three-electrode cell, by using NF as the working electrode, Pt wire as the counter electrode and saturated calomel electrode (SCE) as the reference electrode. The electrolyte was prepared by dissolving 25.0 mmol Ni(NO₃)₂·6H₂O, 5.0 mmol Co(NO₃)₂·6H₂O, and 10.0 mmol Fe(NO₃)₂·6H₂O into 50.0 mL deionized water. Subsequently, the constant potential deposition was performed at -0.60 V vs. SCE for 300 s. After deposition, the NF electrode was rinsed with deionized water, and then sonicated briefly in ethanol and dried in air. The as-obtained electrode was denoted as Ni_{2.5}Co_{0.5}Fe/NF based on the Ni²⁺ : Co²⁺ : Fe³⁺ molar ratio of the precursor electrolyte, and the amount of NiCoFe LDHs electrodeposited on NF was determined to be ca. 0.3 mg cm⁻² by a micro-balance. Similarly, Ni₃Fe/NF and Ni₂CoFe/NF control samples were fabricated in precursor solutions with the same total metal ion concentration but different Ni²⁺ : Co²⁺ : Fe³⁺ ratios.

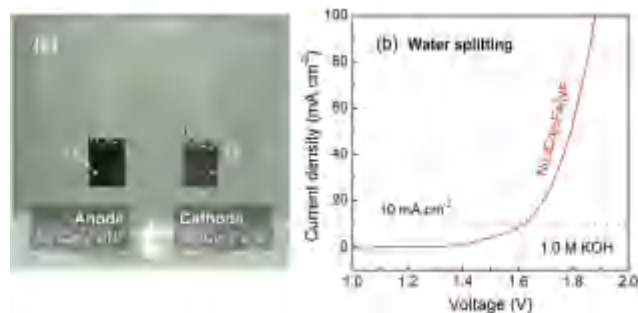


Fig. 4 Two-electrode water electrolysis in a 1.0 M KOH electrolyte. (a) Photograph of the two-electrode configuration using Ni_{2.5}Co_{0.5}Fe/NF as both anode and cathode. (b) Overall water splitting characteristics of the electrolyzer.

Synthesis of NiCoFe LDH samples. A series of NiCoFe LDH samples were synthesized through a facile hydrothermal reaction. In typical synthesis of a Ni_{2.5}Co_{0.5}Fe LDH sample, Ni(NO₃)₂·6H₂O, Co(NO₃)₂·6H₂O, and Fe(NO₃)₂·6H₂O were dissolved into 120 mL deionized water with Ni²⁺, Co²⁺, and Fe³⁺ concentrations of 25.0, 5.0, and 10.0 mmol L⁻¹ respectively. The urea was further dissolved in the solution with a concentration of 0.20 mol L⁻¹ under stirring. After that, the as-obtained slurry was sealed into a 200 mL autoclave and kept at 120 °C for 24 h. After filtering, washing, and freeze-drying, the final product of Ni_{2.5}Co_{0.5}Fe LDH sample was available. As for Ni₃Fe LDH, Ni₂-CoFe LDH, and Ni_{1.5}Co_{1.5}Fe LDH samples, the hydrothermal synthesis was carried out using precursor solutions with the same total metal ion concentration of 40.0 mmol L⁻¹ but different Ni²⁺ : Co²⁺ : Fe³⁺ molar ratios.

Structure characterization

The morphology of the materials were characterized using a JSM 7401F SEM operated at 3.0 kV and a JEM 2010 TEM operated at 120.0 kV. EDS analysis was performed at an acceleration voltage of 120.0 kV using a JEM 2010 TEM equipped with an Oxford Instrument energy dispersive spectrometer. XRD patterns were recorded on a Bruker D8 Advance diffractometer at 40.0 kV and 120.0 mA with Cu-K_α radiation. XPS measurements were carried out by an Escalab 250xi. N₂ adsorption-desorption isotherms at liquid-N₂ temperature were collected using an Autosorb-IQ2-MP-C system, and the specific surface area was calculated based on the multipoint Brunauer-Emmett-Teller method.

Electrochemical measurement

Electrochemical tests were carried out on a three-electrode system controlled by the CHI 760D electrochemistry workstation (CH Instrument, USA). As for the three-electrode system, the NF-based freestanding electrode or a rotating disk electrode (RDE, Pine Research Instrument, USA) with a disk diameter of 5.0 mm was applied as the substrate for the working electrode, with a Pt sheet and a SCE serving as the counter and reference electrodes, respectively. The NiCoFe/NF electrodes as-prepared above were used as the working electrode directly. The NiCoFe LDH samples were tested using the RDE electrode, which was fabricated as follows before each measurement. 5.0 mg NiCoFe LDH sample was firstly dispersed in 0.95 mL ethanol, then 0.05 mL Nafion solution (5.0 wt%) was added, followed by 1.0 h sonication. 10.0 mL suspension was pipetted onto the glass carbon disk electrode, which was mechanically polished and ultrasonically washed in advance. Ultimately, the RDE working electrode with a catalyst loading amount of 0.25 mg cm⁻² was prepared after solvent evaporation in air for 10 min.

OER and HER performance of the catalysts was evaluated by linear sweep voltammetry (LSV) at a scan rate of 10 mV s⁻¹ and room temperature, with the NF-based electrode staying still or RDE rotating at 1600 rpm in the N₂-saturated 0.10/1.0 M KOH electrolyte. Here, 95% iR-compensation was applied for all LSV tests, and the potential versus reversible hydrogen electrode (RHE) was calculated as $E_{vs. RHE} = E_{vs. SCE} + 0.241 + 0.0592pH$.

The electrochemical impedance spectroscopy (EIS) measurement was performed at 0.55 V vs. SCE over a frequency range from 0.10 Hz to 100 kHz at the sinusoidal voltage amplitude of 5.0 mV.

The apparent activation energy for OER was estimated based on LSV measurements at various temperatures. During the test, the electrolytic cell containing 0.10 M KOH was suspended in a thermostatic water bath. The LSV tests were conducted at a scan rate of 10 mV s⁻¹ with 95% iR-compensation. Subsequently, the exchange current density J_0 at each given temperature T was determined from the equation of the Tafel slope,³⁴ with the potential corrected for temperature as $E_{vs. RHE} = E_{vs. SCE} + [0.241 - 6.61 \times 10^{-4}(T - 298)] + 1.98 \times 10^{-4}T$ pH. By plotting $\log J_0$ against $1/T$, the activation energy E_a was calculated according to the Arrhenius equation $v(\log J_0)/v(1/T) = -E_a/2.3R$.^{35,37}

Overall water splitting was performed on a two-electrode system, using Ni_{2.5}Co_{0.5}Fe/NF as both anode and cathode in a 1.0 M KOH electrolyte. The two electrodes were located ca. 2.0 cm away from each other to prevent gas crossover, and the configuration was open to air to release the gas products. And the LSV curves were collected at a scan rate of 10 mV s⁻¹ with 95% iR-compensation.

Acknowledgements

This work was financially supported by the National Natural Science Foundation of China (No. 21306102 and 21422604) and the China Postdoctoral Science Foundation (No. 2015M571049). We also thank Jia-Le Shi and Chen-Yu Chen for their helpful discussion.

Notes and references

- 1 J. A. Turner, *Science*, 2004, 305, 972–974; A. Kudo and Y. Miseki, *Chem. Soc. Rev.*, 2009, 38, 253–278; J. Wang, H. X. Zhong, Y. L. Qin and X. B. Zhang, *Angew. Chem., Int. Ed.*, 2013, 52, 5248–5253.
- 2 Y. Jiao, Y. Zheng, M. Jaroniec and S. Z. Qiao, *Chem. Soc. Rev.*, 2015, 44, 2060–2086.
- 3 K. Zeng and D. Zhang, *Prog. Energy Combust. Sci.*, 2010, 36, 307–326.
- 4 M. G. Walter, E. L. Warren, J. R. McKone, S. W. Boettcher, Q. Mi, E. A. Santori and N. S. Lewis, *Chem. Rev.*, 2010, 110, 6446–6473; Y. Lee, J. Suntivich, K. J. May, E. E. Perry and Y. Shao-Horn, *J. Phys. Chem. Lett.*, 2012, 3, 399–404.
- 5 G. L. Tian, M. Q. Zhao, D. S. Yu, X. Y. Kong, J. Q. Huang, Q. Zhang and F. Wei, *Small*, 2014, 10, 2251–2259; G. L. Tian, Q. Zhang, B. Zhang, Y. G. Jin, J. Q. Huang, D. S. Su and F. Wei, *Adv. Funct. Mater.*, 2014, 24, 5956–5961.
- 6 R. D. Smith, M. S. Prévot, R. D. Fagan, S. Trudel and C. P. Berlinguette, *J. Am. Chem. Soc.*, 2013, 135, 11580–11586; M. Zhang, M. de Respinis and H. Frei, *Nat. Chem.*, 2014, 6, 362–367.
- 7 M. W. Louie and A. T. Bell, *J. Am. Chem. Soc.*, 2013, 135, 12329–12337.

- 8 R. Subbaraman, D. Tripkovic, K.-C. Chang, D. Strmcnik, A. P. Paulikas, P. Hirunsit, M. Chan, J. Greeley, V. Stamenkovic and N. M. Markovic, *Nat. Mater.*, 2012, 11, 550–557; Z. Zhao, H. Wu, H. He, X. Xu and Y. Jin, *Adv. Funct. Mater.*, 2014, 24, 4698–4705; M. S. Burke, M. G. Kast, L. Trotochaud, A. M. Smith and S. W. Boettcher, *J. Am. Chem. Soc.*, 2015, 137, 3638–3648; C. M. Li, M. Wei, D. G. Evans and X. Duan, *Small*, 2014, 10, 4469–4486.
- 9 J. Suntivich, K. J. May, H. A. Gasteiger, J. B. Goodenough and Y. Shao-Horn, *Science*, 2011, 334, 1383–1385; Y. Zhu, W. Zhou, Z. G. Chen, Y. Chen, C. Su, M. O. Tadé and Z. Shao, *Angew. Chem., Int. Ed.*, 2015, 54, 3897–3901.
- 10 D. Kong, J. J. Cha, H. Wang, H. R. Lee and Y. Cui, *Energy Environ. Sci.*, 2013, 6, 3553–3558; D. Merki, H. Vrubel, L. Rovelli, S. Fierro and X. Hu, *Chem. Sci.*, 2012, 3, 2515–2525; J. Wang, H. Zhong, Z. Wang, F. Meng and X. Zhang, *ACS Nano*, 2016, 10, 2342–2348.
- 11 L. Liao, S. Wang, J. Xiao, X. Bian, Y. Zhang, M. D. Scanlon, X. Hu, Y. Tang, B. Liu and H. H. Girault, *Energy Environ. Sci.*, 2014, 7, 387–392; H. Vrubel and X. Hu, *Angew. Chem., Int. Ed.*, 2012, 51, 12703–12706; W. Cui, N. Cheng, Q. Liu, C. Ge, A. M. Asiri and X. Sun, *ACS Catal.*, 2014, 4, 2658–2661.
- 12 E. J. Popczun, J. R. McKone, C. G. Read, A. J. Biacchi, A. M. Wiltrout, N. S. Lewis and R. E. Schaak, *J. Am. Chem. Soc.*, 2013, 135, 9267–9270; P. Jiang, Q. Liu, Y. Liang, J. Tian, A. M. Asiri and X. Sun, *Angew. Chem., Int. Ed.*, 2014, 53, 12855–12859; Q. Liu, J. Tian, W. Cui, P. Jiang, N. Cheng, A. M. Asiri and X. Sun, *Angew. Chem., Int. Ed.*, 2014, 53, 6710–6714.
- 13 H. Wang, H.-W. Lee, Y. Deng, Z. Lu, P.-C. Hsu, Y. Liu, D. Lin and Y. Cui, *Nat. Commun.*, 2015, 6, 7261; C. Tang, N. Cheng, Z. Pu, W. Xing and X. Sun, *Angew. Chem., Int. Ed.*, 2015, 54, 9351–9355; N. Jiang, B. You, M. Sheng and Y. Sun, *Angew. Chem., Int. Ed.*, 2015, 54, 6251–6254; G. Wu, A. Santandreu, W. Kellogg, S. Gupta, O. Ogoke, H. Zhang, H. L. Wang and L. M. Dai, *Nano Energy*, 2016, DOI: 10.1016/j.nanoen.2015.12.032.
- 14 F. Song and X. Hu, *Nat. Commun.*, 2014, 5, 4477; M. Shao, R. Zhang, Z. Li, M. Wei, D. G. Evans and X. Duan, *Chem. Commun.*, 2015, 51, 15880–15893.
- 15 M. Gong and H. Dai, *Nano Res.*, 2015, 8, 23–39; Z. Lu, W. Xu, W. Zhu, Q. Yang, X. Lei, J. Liu, Y. Li, X. Sun and X. Duan, *Chem. Commun.*, 2014, 50, 6479–6482; X. Yu, M. Zhang, W. Yuan and G. Shi, *J. Mater. Chem. A*, 2015, 3, 6921–6928.
- 16 L. Zhou, F. Zhang, T. Zhou, H. Kage and Y. Mawatari, *Korean J. Chem. Eng.*, 2013, 30, 501–507.
- 17 X. Han, C. Yu, J. Yang, C. Zhao, H. Huang, Z. Liu, P. M. Ajayan and J. Qiu, *Adv. Mater. Interfaces*, 2016, 3, 1500782.
- 18 F. Song and X. Hu, *J. Am. Chem. Soc.*, 2014, 136, 16481–16484.
- 19 C. Tang, H. Wang, X. Zhu, B. Li and Q. Zhang, *Part. Part. Syst. Charact.*, 2016, DOI: 10.1002/ppsc.201600004.
- 20 X. Long, S. Xiao, Z. Wang, X. Zheng and S. Yang, *Chem. Commun.*, 2015, 51, 1120–1123; L. Qian, Z. Lu, T. Xu, X. Wu, Y. Tian, Y. Li, Z. Huo, X. Sun and X. Duan, *Adv. Energy Mater.*, 2015, 5, 1500245.
- 21 Z. Lu, L. Qian, Y. Tian, Y. Li, X. Sun and X. Duan, *Chem. Commun.*, 2016, 52, 908–911.
- 22 M. Gong, Y. Li, H. Wang, Y. Liang, J. Z. Wu, J. Zhou, J. Wang, T. Regier, F. Wei and H. Dai, *J. Am. Chem. Soc.*, 2013, 135, 8452–8455.
- 23 X. Long, J. Li, S. Xiao, K. Yan, Z. Wang, H. Chen and S. Yang, *Angew. Chem., Int. Ed.*, 2014, 53, 7584–7588; C. Tang, H. S. Wang, H. F. Wang, Q. Zhang, G. L. Tian, J. Q. Nie and F. Wei, *Adv. Mater.*, 2015, 27, 4516–4522; X. Zhu, C. Tang, H.-F. Wang, Q. Zhang, C. Yang and F. Wei, *J. Mater. Chem. A*, 2015, 3, 24540–24546.
- 24 D. Tang, J. Liu, X. Wu, R. Liu, X. Han, Y. Han, H. Huang, Y. Liu and Z. Kang, *ACS Appl. Mater. Interfaces*, 2014, 6, 7918–7925.
- 25 Z. Lu, Y. Li, X. Lei, J. Liu and X. Sun, *Mater. Horiz.*, 2015, 2, 294–298.
- 26 M. Gong, W. Zhou, M. J. Kenney, R. Kapusta, S. Cowley, Y. Wu, B. Lu, M. C. Lin, D. Y. Wang, J. Yang, B. J. Hwang and H. Dai, *Angew. Chem., Int. Ed.*, 2015, 54, 11989–11993.
- 27 J. Liang, R. Ma, N. Iyi, Y. Ebina, K. Takada and T. Sasaki, *Chem. Mater.*, 2009, 22, 371–378; J. Yang, C. Yu, X. Fan and J. Qiu, *Adv. Energy Mater.*, 2014, 4, 1400761.
- 28 T. Yamashita and P. Hayes, *Appl. Surf. Sci.*, 2008, 254, 2441–2449; P. C. Graat and M. A. Somers, *Appl. Surf. Sci.*, 1996, 100, 36–40; X. Lu and C. Zhao, *Nat. Commun.*, 2015, 6, 6616.
- 29 C. Tang, H.-F. Wang, H.-S. Wang, F. Wei and Q. Zhang, *J. Mater. Chem. A*, 2016, 4, 3210–3216.
- 30 C. C. McCrory, S. Jung, J. C. Peters and T. F. Jaramillo, *J. Am. Chem. Soc.*, 2013, 135, 16977–16987.
- 31 N. Danilovic, R. Subbaraman, D. Strmcnik, K. C. Chang, A. Paulikas, V. Stamenkovic and N. M. Markovic, *Angew. Chem., Int. Ed.*, 2012, 51, 12485–12498.
- 32 J. Luo, J.-H. Im, M. T. Mayer, M. Schreier, M. K. Nazeeruddin, N.-G. Park, S. D. Tilley, H. J. Fan and M. Grätzel, *Science*, 2014, 345, 1593–1596.
- 33 A. Audemer, A. Delahaye, R. Farhi, N. Sac-Épée and J. M. Tarascon, *J. Electrochem. Soc.*, 1997, 144, 2614–2620; V. Pralong, A. Delahaye-Vidal, B. Beaudoin, J. B. Leriche and J. M. Tarascon, *J. Electrochem. Soc.*, 2000, 147, 1306–1313.
- 34 J. R. Swierk, S. Klaus, L. Trotochaud, A. T. Bell and T. D. Tilley, *J. Phys. Chem. C*, 2015, 119, 19022–19029; M. Miles, G. Kissel, P. Lu and S. Srinivasan, *J. Electrochem. Soc.*, 1976, 123, 332–336.
- 35 L. M. Da Silva, D. V. Franco, L. A. De Faria and J. F. Boodts, *Electrochim. Acta*, 2004, 49, 3977–3988.
- 36 S. Chen, J. Duan, P. Bian, Y. Tang, R. Zheng and S. Z. Qiao, *Adv. Energy Mater.*, 2015, 5, 1500936; H.-F. Wang, C. Tang and Q. Zhang, *J. Mater. Chem. A*, 2015, 3, 16183–16189.
- 37 S. Jasem and A. Tseung, *J. Electrochem. Soc.*, 1979, 126, 1353–1360.